International Journal of Nanoelectronics and Materials

In Press, Accepted Manuscript – Note to user

Q-switched Nd: YAG fundamental and second harmonic wavelengths impact on preparing Nb_2O_5 thin films by a PLD technique: a comparative study

Suhair R. shafeeq[1], Evan T. Salim[1,*], Mohammed Jalal AbdulRazzaq[1]

[1] Laser and Optoelectronic Department, University of Technology-Iraq, Baghdad, Iraq.
[2]Applied Science Department, University of Technology-Iraq, Baghdad, Iraq

Received 27 April 2022, Revised 13 October 2022, Accepted 31 October 2022

ABSTRACT

We aim to study and investigate the structural, optical, topographical, and morphological properties of Nb_2O_5 thin films deposited under vacuum Q-switched Nd: YAG pulsed laser for the first time for the best of our knowledge. The obtained results of this study can contribute in different fields of applications including the optoelectronic and biomedical fields. The fundamental (1064 nm) and the visible second harmonic (532 nm) wavelengths were utilized for this purpose. The laser energy was fixed at 657 mJ. The number of pulses and the substrate temperatures were 200 laser shots and 450 ºC, respectively. The observed X-ray diffraction patterns were assigned for T-Nb_2O_5 that refers to the orthorhombic and H-Nb_2O_5 which is related to the monoclinic phases supported by Raman spectra analyses. Nb_2O_5 thin film deposited by Nd: YAG fundamental wavelength (1064nm) showed a thicker film, a higher surface roughness and, on average, a larger particles size It also provided better matching of the lattice d-spacing with the standard d-spacing obtained by JPCDs cards 00-030-0873 and 00-009-0372. The optical properties including the band gap values for both direct and indirect transitions were estimated with the lower gap was reported for the thin film prepared at the fundamental wavelength. The photoluminescence analyses supported that the transitions of both prepared films were indirect. FE-SEM clarified the surface morphology of each prepared film. The EDX analyses provided the elemental compositions and the purity of the Nb_2O_5 prepared films.

Keywords: ad-atoms, monoclinic, octahedral, PLD, second harmonic.

1. INTRODUCTION

Pulsed laser deposition technique (PLD) is one of the preferable methods for preparing and growing thin films and nanostructures. Since 1980s up to the latest decade, there have been more than a thousand of published items about pulsed laser deposition technique[1-3]. A wide range of materials can be deposited by this technique[4, 5].

Thin films can also be simply and rapidly grown with high and desirable qualities [6]. Different lasers of different wavelengths have been used to ablate a circularly pressed nanomaterial powder onto a chosen substrate. KrF, λ=248 nm, has been mostly used in pulsed laser deposition technique [7, 8]. Despite the fact that excimer lasers provide more stabilized energy than Nd:YAG

*For correspondence; Tel. + (964) 7715752087, E-mail: evan_tarq@yahoo.com, & 100354@uotechnology.edu.iq.

laser[9], but it provides a higher hazardous environment for the user due to the existence of species[4, 10]. Different materials can be obtained by Nd: YAG laser radiation with the fundamental, second and third harmonic wavelengths. Nb_2O_5 is the one of these materials. Nb_2O_5 is a member of the transition metal oxides[11-12] with different oxidation states such as NbO, NbO_2, Nb_2O_3 and Nb_2O_5. It is an n-type semiconductor material possessing a band gap range of 3.1 eV (semiconductor) to 5.3 eV (insulator). Nb_2O_5 is the most thermodynamic stable form among all the defined oxidations states of Nb-O systems[13-15]. In recent decades, thin films and nanostructures of Nb_2O_5 has attracted a great attention due to the prominent features such as a wide band gap, anti-corrosion, insoluble in air, excellent biocompatible, not cytotoxic [16-17], and well-adhesive material[18, 19].These features contributed to utilize Nb_2O_5 in applications such as sensors, solar cells, eletrochromic devices, supercapacitors, catalyst [8–11] and medical applications[12–14].

PLD method was not extensively employed to fabricate Nb_2O_5 thin films, therefore more studies as well investigations are required to understand its behavior under pulsed laser technique [28]. In addition, the laser pulse photon energy plays a vital role in modifying the thin film properties including the particle size, the film's periodicity, the surface morphology, and the surface roughness which are all regarded as important factors in nanomaterial science. Furthermore, changing the laser photon energy simply by using a second, third, or fourth harmonic wavelengths can considerably influence and modify the deposited thin films to be incorporated in a vast range of applications. The third harmonic Nd: YAG pulsed laser wavelength was used to fabricate Nb_2O_5, among other niobium oxides, in 1999 by Fu et. al.[29]. The aim of the researcher was to investigate the electrochemical and electrochromic properties of Nb_2O_5 thin films by PLD with a background gas [30]. The fundamental wavelength of Nd:YAG laser was used in 2021 by Fakhri et al.[31] to investigate the post-deposition annealing temperature influence on Nb_2O_5 films' physical properties in a vacuum with 0 pressure.

In this work, we aim to study the effects induced by both fundamental and second harmonic Q-switched Nd: YAG pulsed laser wavelengths on Nb_2O_5 thin films for the first time. Structural, optical, topographical, morphological, and properties were investigated under fixed parameters. These parameters including the laser energy that was kept at 657 mJ, the substrate temperature of 450 ºC, and 200 laser shots in 10^{-3} mbar as a vacuum pressure. Studying these properties of Nb_2O_5 thin films under two laser wavelengths can lead to different results via a single process that the characteristics of each prepared Nb_2O_5 thin film can be desirable in specific applications.

2. MATERIAL AND METHODS

Quartz substrates were cleaned for the purpose of contaminants removal. An ultrasonic device was filled with a mixture of deionized water and ethanol for more than fifteen minutes was utilized for the cleaning purpose. Nb_2O_5nano powder from Merck (Kenilworth, NJ) with a purity of 99.99% was pressed under twelve tons pressure producing a circular-like shape target with a diameter of 2.5 cm and a height of 0.5 cm. Nd: YAG laser with the fundamental wavelength (1064 nm) was firstly used to prepare Nb_2O_5 thin films. The second harmonic wavelength (532 nm) was then separately utilized to deposit Nb_2O_5 thin film. All the parameters, except the laser wavelength, were fixed in order to study and investigate the differences in the obtained films. The PLD system employed for the deposition process is shown in Figure1.

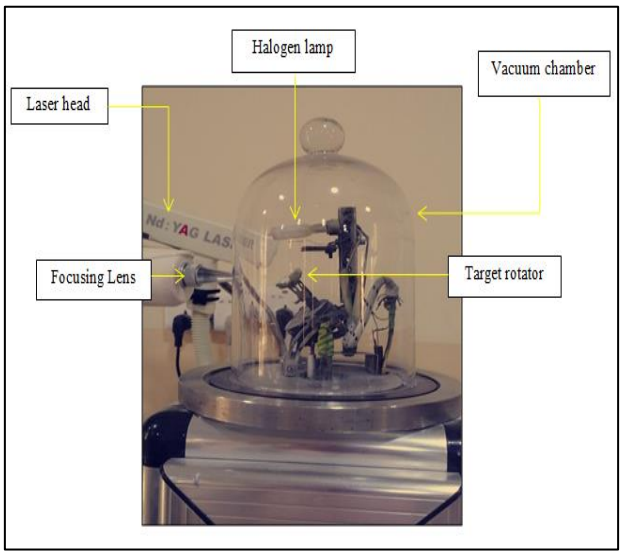

Figure 1. pulsed laser deposition system.

The pulsed laser energy was selected at 657 mJ. The focal length was 12 cm. The substrate was heated to450 ºC by a halogen heater that was built-in the PLD system. The number of laser pulses was only (200 shots) with a frequency of 3 Hz and pulse duration of 10 ns.

The separation between the laser and the target was about 10 cm, while the target and the substrate were spaced by 3 cm. The vacuum pressure inside the chamber was kept at 10^{-3} mbar. A lens was used for depositing Nb_2O_5 thin film with Q-switched Nd: YAG laser fundamental wavelength in order to focus the incident radiation onto a small area of the target surface. For depositing Nb_2O_5 with the second harmonic wavelength, a KDP crystal was employed to generate 532 nm as a second harmonic. Both of the lens and the crystal utilized in the deposition process are shown in Figure2.

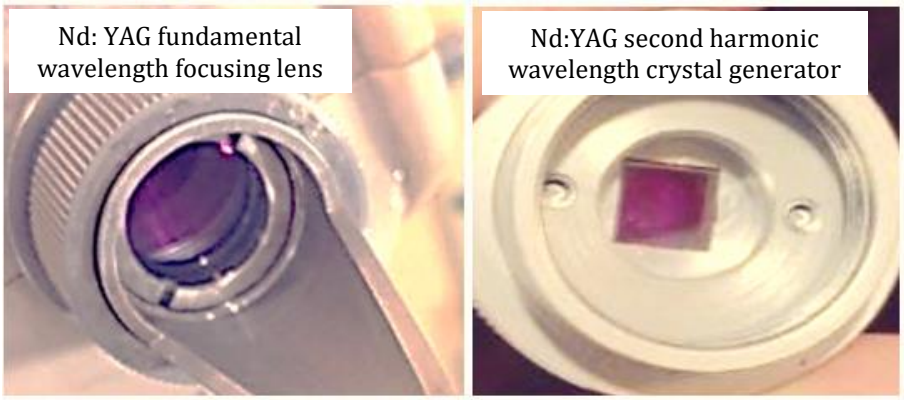

Figure 2. fundamental wavelength lens and second harmonic generator crystal of Nd: YAG laser.

3. Nb_2O_5 THIN FILM CHARACTERIZATIONS AND MEASUREMENTS

The structures of the obtained films were analysed by the X-ray diffractometer device using DANDONG HAOYUAN DX-2700B XRD equipped with Cu-kα radiation source. The crystallite size of the predominant peaks was calculated by Scherrer's equation [32-33]:

$$D_{XRD} = \frac{k\lambda}{\beta * \cos(\theta)} \text{ (nm)} \quad (1)$$

Where (D) is the crystallite size, (K) is constant (0.94), (λ) is the exciting X-ray wavelength, (β) is the FWHM and (θ) is half angle position between the incident and the scattered wavelength.
The dislocation densities (δ) were also calculated by [34-35]:

$$\delta = \frac{1}{D^2} \quad X\ 10^3 \text{ (line.cm}^{-1}\text{)} \quad (2)$$

The microstrain (ε) of prepared films were calculated by Wilson formula [36-37]:

$$\varepsilon = \frac{\beta}{4\tan\theta} \quad X\ 10^3 \quad (3)$$

Each prepared thin film's thickness (t) was obtained by Fizeau optical interference [38, 39] using a He-Ne laser source and a beam expander.

$$t = 316.4\ \frac{\Delta x}{x} \quad (4)$$

Where (x) is the width of the bright fringe and (Δx) is the spacing between two consecutive fringes that results from destructive interference.
In addition to XRD analyses, Raman spectrometer from SUNSHINE (version V2-86) was used to provide a further investigation of Nb_2O_5 structures and molecular behaviour. A double-beam UV-VIS (SHIMADZU, 1800) spectrophotometer was utilized to collect the absorption data. Photoluminescence from FIRMWARE (version: 131024, serial No. F-S 1401004) was used to understand the emissions of the prepared films and the related band gaps. By the UV-visible data, the optical absorption coefficients (α) as function of excitation ratio were calculated by using [40, 41]:

$$\alpha = \frac{2.303A}{t} \text{ (cm}^{-1}\text{)} \quad (5)$$

Where (A) is the absorption percentage.
The extinction coefficients for each prepared film were given by [42-43]:

$$k = \frac{\alpha\lambda}{4\pi} \quad (6)$$

The incident photon energy (Eg) was calculated by [44-45]:

$$E_g = \frac{1240}{\lambda} \text{ (nm)} \quad (7)$$

The optical band gap values were obtained by Tauc's equation [46-47]:

$$(\alpha h\nu) = B(h\nu - Eg)^{1/r} \quad (8)$$

Where (h) is Planck's constant, (ν) is the frequency of the incident photon, (B) is constant that is the band tailing parameter, (r) is a constant with different values based on the material type transitions.
The atomic force microscopy (AFM) TT-MODEL was used to investigate each prepared thin film surface roughness. The obtained films were also tested by the field emission scanning electron microscopy (FE-SEM) from MIRA3 TESCAN and the energy dispersive X-ray analyses (EDX) to investigate the morphological properties and the chemical compositions, respectively.

4. RESULTS AND DISCUSSION

4.1 STRUCTURAL PROPERTIES

Generally, the nanoparticle size and the material behaviour under the laser wavelength impact showed unclear patterns. Previous studies [48-50] of various materials showed different results related to the films behaviours, therefore the laser wavelength impact is still not fully investigated. In this study, the XRD profile, shown in Figure 3, indicated for the polycrystalline structures of Nb_2O_5 thin films prepared by both the fundamental and the second harmonic Nd: YAG laser wavelengths. Orthorhombic (T-Nb_2O_5) and monoclinic (H-Nb_2O_5) phases were obtained according to the JPCDS card No. (00-030-0873) and (00-009-0372), respectively. For the film prepared at 1064nm, the observed peaks were centred at the angles' positions (2θ) of 22.6º, 26.2º, 28.8º, 35.2º and 36.1º with miller indices (hkl) of (0 0 1), (4 0 2), (2 0 0), (3 1 3) and (2 0 1), respectively.

.

On the other hand, the thin film obtained by Nd:YAG second harmonic wavelength showed some differences. Orthorhombic (T-Nb_2O_5) and monoclinic (H-Nb_2O_5) were also obtained. However; an additional peak centred at (2θ) equals to 56° belonged to (T-Nb_2O_5) was also obtained. The peaks positions (2θ) were at 26º, 28.4º, 38.4º, 46.8º and 56.4º and the related miller indices were (4 0 2), (1 8 0), (-9 0 3), (0 0 2) and (3 8 1). Similar indication was found in ref [51]. The predominant peaks were at angles' positions of (28.8º) and (28.4º) with different orientations. The broadened peak positioned at the angle (28.4º) was due to the small particle size obtained by the second harmonic generation Nd:YAG laser wavelength, as they will be confirmed by AFM and FE-SEM scanning results.

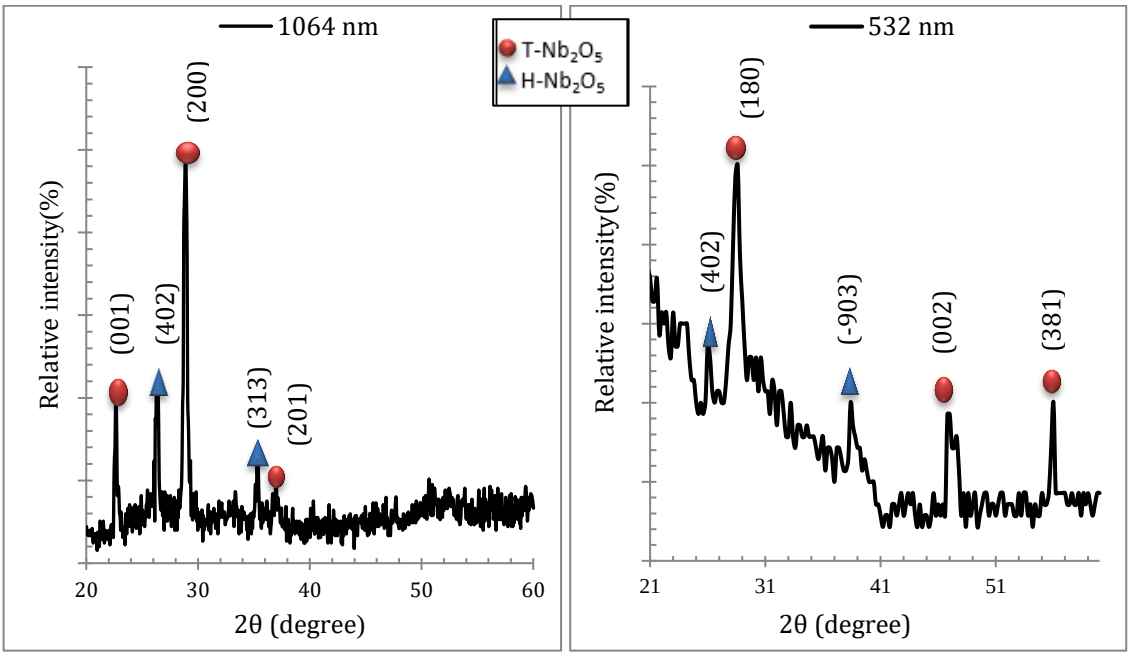

Figure 3. the XRD diffraction profile for Nb_2O_5 thin films prepared by the fundamental (1064nm) and te second harmonic wavelength (532 nm).

The lattice d-spacing of the obtained films deposited by both wavelengths in comparison with the standard values are shown in Figure 4. Expectedly, and according to the discussion above, Nb_2O_5 prepared film by the fundamental wavelength provided better matching with the standard d-spacing values than the film deposited by 532 nm wavelength.

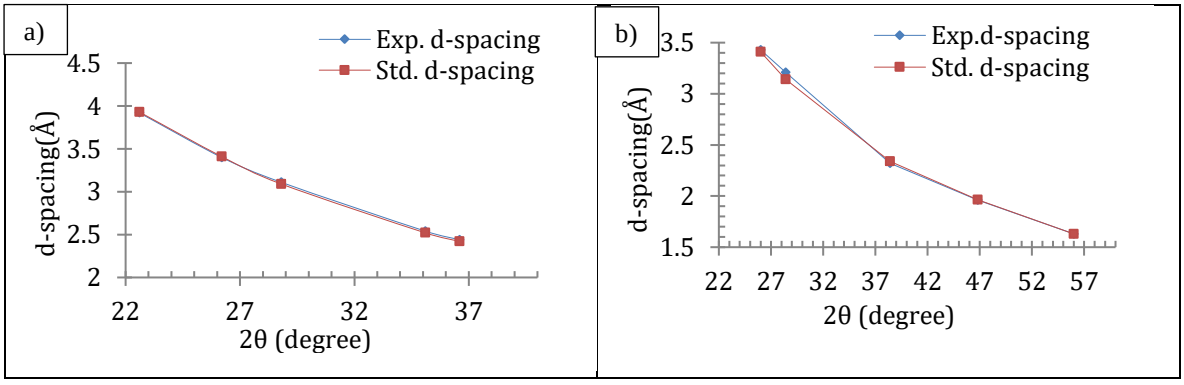

Figure 4. Lattice d-spacing in comparison with the standard lattice d-spacing of the obtained T-Nb_2O_5 and H-Nb_2O_5 by Nd:YAG laser at both (a)1064, and (b) 532 nm.

The full widths at half maxima, dislocation densities, microstrain and stress values for the prepared films are listed in Table1. As a known fact, small particles refer to higher dislocation densities and a higher exposure to microstrain and stress. This is because better stacking can be obtained with the larger particles as compared with the smaller ones.

Table 1. the FWHM, the obtained d-spacing, crystallites' size, dislocation densities and microstrain of Nb_2O_5films prepared by the fundamental (1064 nm) and the second harmonic (532 nm) wavelengths.

Laser wavelength (nm)	2θ (degree)	FWHM (degree)	d-spacing (Å)	D (nm)	δ *10³	ε *10³
1064	22.6	0.46	3.92	17.68	3.19	0.40
	26.2	0.38	3.40	21.27	2.20	0.38
	28.8	0.30	3.11	25.12	1.38	0.33
	35.1	0.29	2.54	27.28	1.34	0.40
	36.6	0.32	2.44	24.36	1.64	0.46
532	26.0	0.71	3.43	11.3	7.70	0.71
	28.4	0.85	3.21	9.46	11.7	0.93
	38.4	0.99	2.32	7.92	15.9	1.50
	46.8	1.39	1.96	5.48	33.2	2.62
	56.0	0.64	1.63	4.50	49.3	3.77

Well-stacked layers of large particles impact on the X-ray diffractions that show more regular patterns and narrower peaks' widths. Pulsed laser wavelength plays a significant role in the absorption process by the target material. The photon-electron interaction leads to a localized thermal impact hence, the ejection mechanism of the material [52]. This thermal impact led the longer wavelength to cause a larger ejection of the material target, hence larger deposited particles onto the substrate. Bothe laser shots of the fundamental and the second harmonic wavelengths are illustrated in Figure 5. Obviously, the zone ablated via higher photon energy (the second harmonic wavelength of 532 nm) led to a superficial ejection easier ejection mechanism) from the target outermost layer, while the zone irradiated by the fundamental (1064 nm) was in smaller area due to lower photon energy

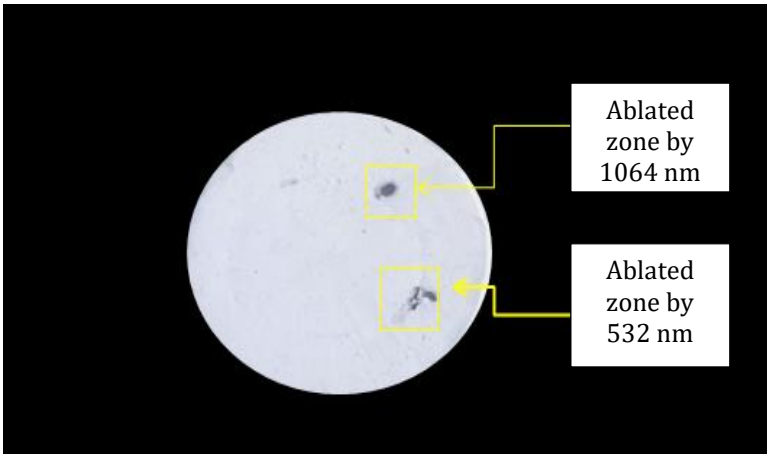

Figure 5. Nb_2O_5 target with the fundamental and the second harmonic laser shots

4.2 TOPOGRAPHICAL ANALYSES

Table 2 summarizes the estimated thickness as well as the surface root mean square and the average roughness' for prepared films at both fundamental and second harmonic Nd:YAG pulsed laser wavelengths. The film's thickness deposited by the second harmonic wavelength of the Q-switched pulsed Nd:YAG laser was less than the film's thickness prepared by the fundamental wavelength by approximately 39.7nm.

Table 2. films' thickness', RMS roughness and average roughness for Nb2O5 thin films prepared by Nd:YAG laser fundamental and second harmonic laser wavelengths.

Laser wavelength (nm)	Photon energy (eV)	Film Thickness (nm)	RMS roughness (nm)	Average roughness (nm)
1064	1.16	116.1 ±1	3.12	2.29
532	2.33	76.4 ±1	1.67	1.24

The decreased size of the particles of Nb_2O_5 thin film deposited by the second harmonic laser wavelength led to lower RMS and average roughness values. The topographical images and the related histograms of the films prepared by both the fundamental and the second harmonic Nd:YAG laser wavelengths are shown in Figure 6. The maximum particles' heights, as shown in the related histogram, obtained by the fundamental laser wavelength were about 100.3 nm, while the maximum height of the particles deposited by 532nm reported 61.6 and nm. Similar indication of surface roughness obtained by Nd: YAG fundamental and second harmonic laser wavelengths were found elsewhere [53]. Figure 7 a –b shows the homogeneous distributions of the particles. It can be clearly observed that Nb_2O_5 thin film prepared by the fundamental wavelength show larger particles than Nb_2O_5 thin film prepared by the second harmonic wavelength. Nb_2O_5 thin films' histograms illustrate the number of scanned particles as a function of the particle size. Nb_2O_5 thin film prepared by the fundamental laser wavelength shows that the average particle size is about 64.7 nm, while the histogram of Nb_2O_5 thin film prepared by the laser second harmonic wavelength shows that the average particle size is 43.6 nm.

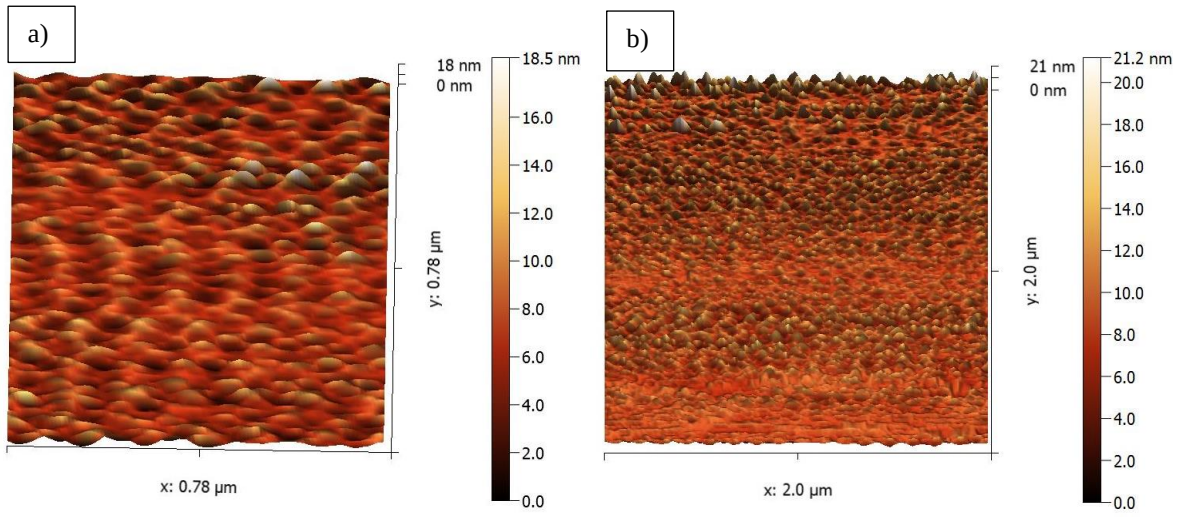

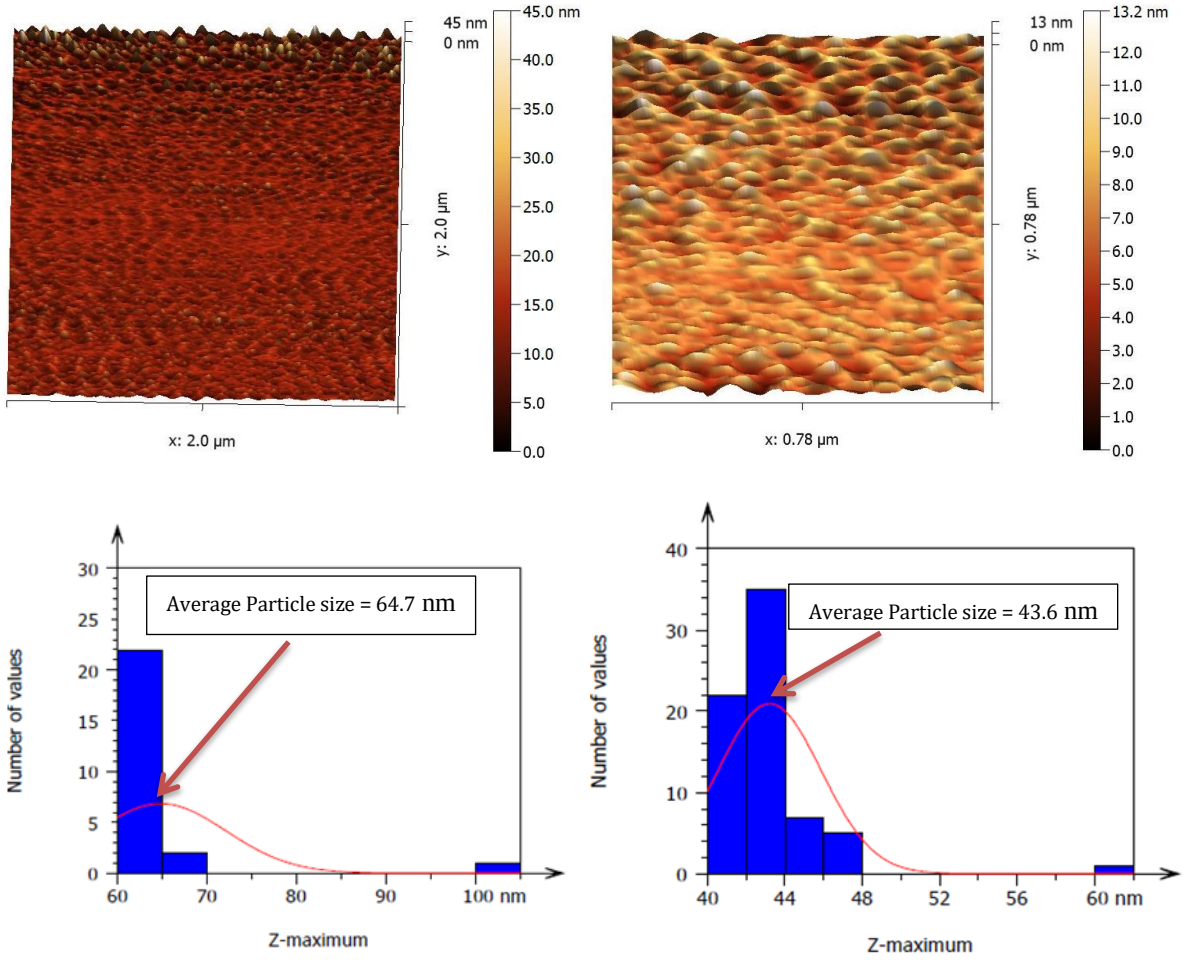

Figure 6. Topographic images and the related histograms for Nb_2O_5 prepared films by Nd: YAG pulsed laser wavelengths with (a) fundamental wavelength. (b) second harmonic wavelength.

4.3 OPTICAL PROPERTIES

Considering the optical properties, the band gap estimation provides the most significant optical property of thin films. The UV-visible spectrophotometer data, Figure 7, showed each deposited film's absorbance as a function of a wavelength range. The fundamental wavelength prepared Nb_2O_5 thin film possessed a higher absorbance than the film obtained by the second harmonic wavelength, as shown in Figure 7-b. According to Beers-Lambert law, the thicker surface contributes in a lower transmission and a higher absorption. In addition, the larger nanoparticles of the film prepared at 1064 nm supported the higher absorption value. Despite the fact that pulsed Nd: YAG double-frequency laser has a higher photon energy, however, a deep ablation does not occur in contrast with the fundamental frequency (photon). Taucs' plots for both direct and indirect allowed transitions were employed to estimate the obtained films' band gaps. The direct band gap value was about 4.7 eV for the film prepared by the fundamental wavelength, while it was estimated to be 5 eV for the film fabricated by 532nm wavelength. The indirect optical band gap values were 2.9 and 3.1 eV, respectively.

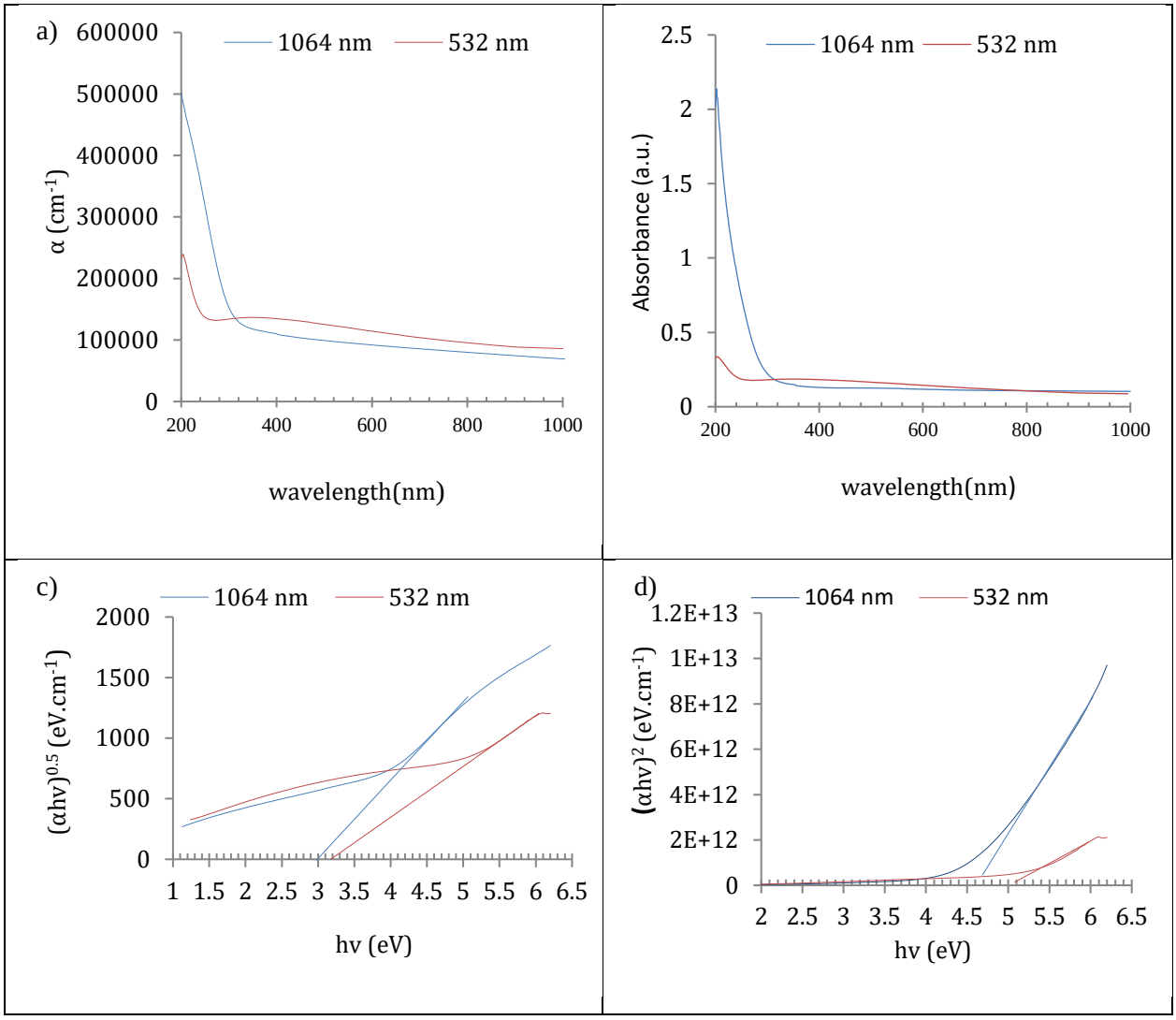

Figure 7. Nb_2O_5 thin films prepared by the fundamental and the second harmonic laser wavelengths.(a) the absorption coefficients. (b) the absorbance values. (c) Tauc's plot for indirect allowed transitions. (d) Tauc's plot for direct allowed transitions.

Table 3 provides the cut-off wavelengths and the calculated optical band gap values for Nb_2O_5 films deposited by 1064nm and 532 nm. The cut off wavelengths were observed from the absorption edge, Figure 7-b, of each prepared film. Both of the deposited films at different wavelengths showed a transparency in the visible region of spectrum. The higher absorbance of Nb_2O_5 thin film prepared by the fundamental wavelength showed a higher cut off wavelength than the film prepared by the second harmonic laser wavelength due to the higher absorption coefficient in the UV region of the former.

Table3. direct and indirect band gap values and cutoff wavelengths for deposited films by the fundamental (1064nm) nm and the second harmonic (532 nm) Nd:YAG laser wavelengths.

Deposition wavelength (nm)	Direct band gap (eV)	Indirect band gap (eV)	λ_{cutoff} (nm)

1064	2.9	3.1	269
532	4.7	5.0	254

The extinction coefficient is a measure of the scattering losses in the material. Figure 8 illustrates the extinction coefficients of both prepared films. The lower (k) value in the visible region of the spectrum for the film prepared at the fundamental wavelength indicates for a higher transparency in the visible region (opaque in the UV region of the spectrum) that is related to the lower optical density (absorption coefficient) in that region.

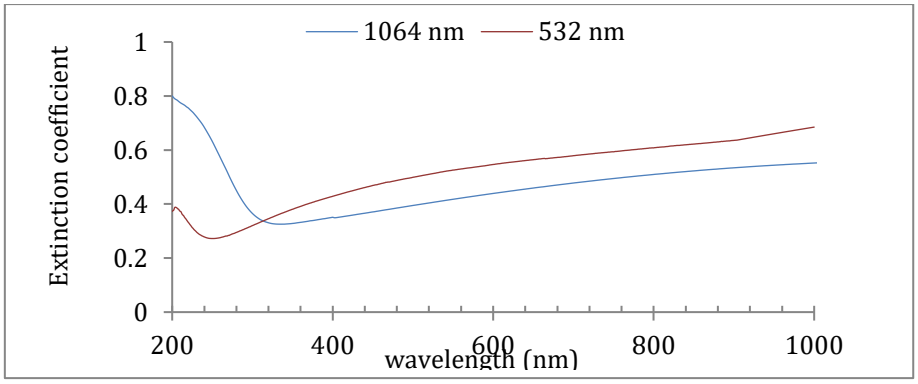

Figure 8. the extinction coefficients (k) for the prepared films by both the fundamental (1064 nm) and the second harmonic wavelength (532 nm).

Prepared Nb_2O_5 thin films were also tested by PL analyses, shown in Figure 9, to understand the emission behaviour at certain wavelengths and to support the data provided by the UV-Visible spectrophotometer. The excitation wavelength was at 320 nm and the emissions were begun at 330 nm for both prepared thin films. Emission peaks at the UV and the visible range of the wavelength spectrum were observed. For the film deposited by the fundamental wavelength, ultraviolet emissions were due to the near band edge (emission from the conduction band lowest state to the highest state of the valence band). Oxygen vacancies also caused internal transitions within the band gap that interpret the observed emissions at 460.5 and 474.1 nm for both fundamental and second harmonic wavelengths that employed in the deposition process, respectively. The optical band gap observed at the intense UV emission for 532 nm prepared film (3.1 eV), while the visible emission at 417 nm indicated to the optical band gap of (3 eV) for prepared film at the fundamental wavelength. Higher intensity of the film synthesized at 532 nm may belong to the non-radiative recombination centres that are created by the distorted octahedral leading to oxygen deficiencies within the band gap. PL analyses well agreed with the indirect band gap values estimated by Tauc's plot. However, the noticed PL peaks' broadening could be related to the phonon interaction that is obviously occurred in the indirect transitions. Similar indications were found by ref [54, 55] with a close emission range.

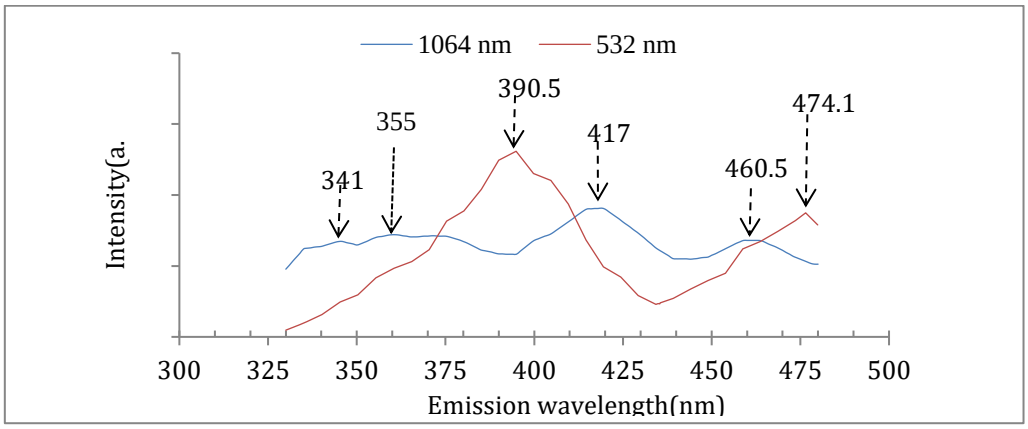

Figure 9. PL analyses for Nb_2O_5prepared films by Nd:YAG pulsed laser fundamental and second harmonic wavelengths.

4.4 RAMAN MOLECULAR BONDS ANALYSES

Nb_2O_5 prepared thin films were also tested by Raman spectra to further investigate the films' structures and to support the information provided by the XRD profile. As illustrated in Figure10, few bands were observed for both prepared Nb_2O_5 films. The bands located at 110.6 and 190.5 cm^{-1} (within the low wavenumber range) are commonly observed in metal oxides. A weak band, with a bending mode, was appeared at 291 cm^{-1} referring to (H-Nb_2O_5) within the same range indicated by ref [56, 57]. The bands observed at 689.7 and 645.7 cm^{-1} proved the orthorhombic phase structure of Nb_2O_5 thin films prepared by the fundamental (1064 nm) and the second harmonic (532 nm) wavelengths, respectively, also indicated by ref [58]. Another observed band at 397.1 cm^{-1} referred to the monoclinic (H-Nb_2O_5). A weak band at 1016 cm^{-1} was observed. The octahedral distortion can result in both shared-edge and corner-edge bands with higher intensity of edge-shared octahedra hence, it supports the estimation of a weak shared-edge octahedra rather than a corner-shared octahedra at this band (1016 cm^{-1}). The higher intensity of Nb_2O_5 synthesized by the second harmonic Nd: YAG laser wavelength with more uniform stretching band was due to the intense compression of the molecule due a slight irregularity in the formed lattice, revealed by the obtained d-spacing as compared with the standard d-spacing. That caused more compression of the molecule, hence a higher intense band was observed. In addition, the broader bands of the film prepared by 532 nm may be caused by smaller particles with higher dislocation densities. These results are in a good agreement with the XRD profile.

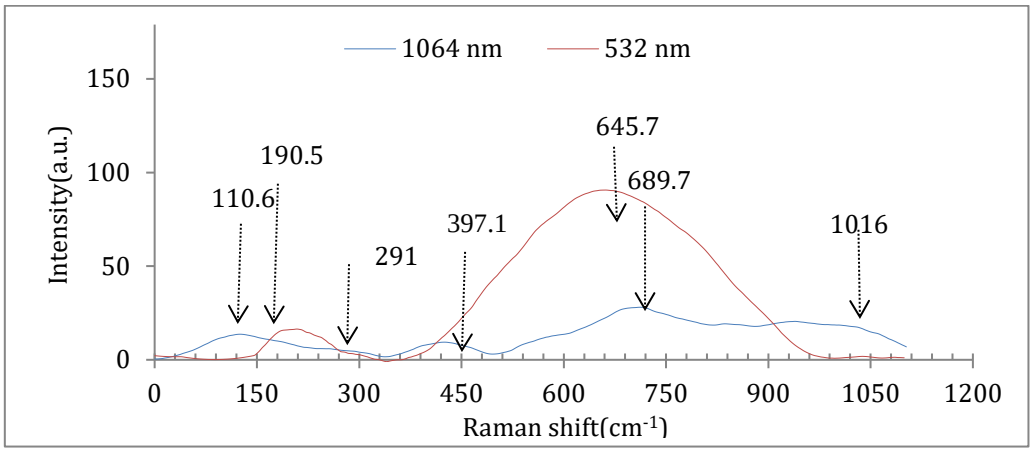

Figure 10. Raman spectra for Nb_2O_5 prepared films by Nd:YAG fundamental and second harmonic wavelengths.

4.5 MORPHOLOGICLA DESCRIPTION AND EDX ANALYSES

Figure11 a-b illustrates the morphological description and EDX analyses (find a better word) of Nb_2O_5 prepared films. The thin film formed by employing the fundamental (1064 nm) wavelength showed clear defined particles and the boundaries were clearly observed. However, more spherical particulates are observed on the surface of the film prepared by the fundamental wavelength than the film prepared by the second harmonic wavelength. These particulates are normally occurred due to the thermal shockwaves induced by the fundamental wavelength of Nd:YAG laser. The smaller particles obtained from 532 nm wavelength (high photon energy) refer to the fragmentation process when the laser photon interacts with the target material. To explain that, as Nb_2O_5 is a molecular compound of Nb and O, the molecular bonds are impacted by the laser wavelength as well as the pulse duration. When Q-switched Nd:YAG pulsed laser with its long fundamental laser wavelength (1054 nm) and pulse duration of few nanoseconds is employed to irradiate Nb_2O_5 target, the vibrational states of the molecules are impacted and photo-ionization process can be occurred and plasma generation was occurred with a high temperature (as a result of inverse Bremsstrahlung process). In other words, a long laser wavelength can induce thermal shockwaves that large species are photo-ionized and ablated. On the other hand, the shorter wavelength (higher photon energy) of the second harmonic pulsed laser is highly absorbed via the electronic states of the material with less thermal shockwaves, thus a fragmentation process is expected [5], [58-59].

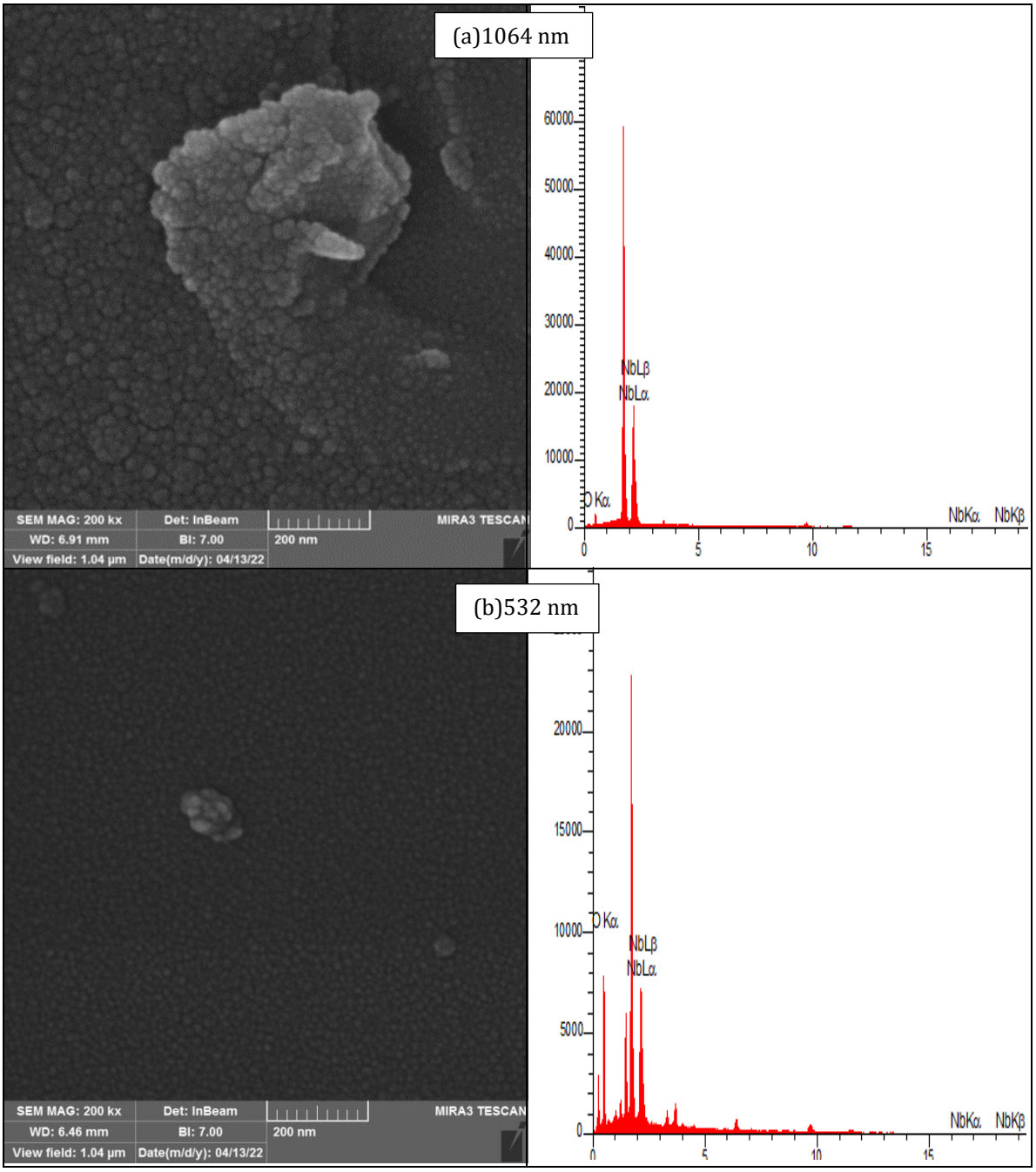

Figure 11. morphological graphs of the prepared films by (a) the fundamental (1064 nm) and (b) the second harmonic wavelength (532 nm).

Table4 provides the chemical compositions of the prepared films with the related weights and the scanned samples by the EDX instrument. Both films provided a high purity with Nb/O ration is higher for the film prepared by 532 nm. This can be justified by the lower number of particulates formed on the surface of the film prepared by 532 nm.

Table 4. elemental chemical compositions and their weights percentages detected by EDX for prepared films by the fundamental (1064 nm) and the second harmonic (532 nm) laser wavelengths.

Deposition wavelength (nm)	Nb wt. %	O wt. %	Nb/O ratio
1064	68.95	31.05	2.22
532	70.67	29.33	2.41

5. CONCLUSION

XRD profile showed that orthorhombic (T-Nb_2O_5) and monoclinic (H-Nb_2O_5) phases were obtained supported by Raman spectroscopic analyses. The optical properties showed that Nb2O5 thin film prepared by the fundamental nm possessed a higher absorbance and lower optical (direct and indirect) band gaps. The PL analyses supported the Tauc's plot estimations for the optical band gaps and showed a well agreement with the indirect band gap values. Larger particles were obtained for the film prepared by the fundamental wavelength of Nd: YAG pulsed laser with a higher surface roughness supported by the AFM topographical views of the tested samples. Surface morphological micrographs of both samples supported the AFM analyses. Both of the deposited films by the fundamental and the second harmonic Nd: YAG pulsed laser wavelengths showed pure structures with a higher Nb/O ratio belonged to the film prepared by the second harmonic Nd: YAG pulsed laser wavelength. Both of Nb_2O_5 thin films prepared by the fundamental and the second harmonic laser wavelengths can be exploited in different applications due to different particles' sizes of both thin films. For example, as Nb_2O_5 thin film prepared by the fundamental laser wavelength showed larger particle size and higher thickness, it can be used in optoelectronic applications as more atoms can attribute in electrical conductivity. Lower absorbance in visible region qualifies Nb_2O_5 thin film prepared by the second harmonic wavelength to be exploited in medical applications such as to increase the microhardness of the dental implants that smaller nanoparticles induce a higher hardness.

ACKNOWLEDGEMENTS

The authors would like to thank the University of Technology for the logistic support this work.

REFERENCES

[1] Lorenz, M., Rao, M. S. R., J. Phys. D. Appl. Phys., vol. **47**, issue 3 (2013) p. 30301.
[2] Abood, M. K., Salim, E. T., Saimon, J. A., Hadi, Aseel A., International Journal of Nanoelectronicsand Materials, vol. **14**, issue 3 (2021) pp. 259-268.
[3] Knez, B. C., Mondal, D.C., Chaluvadi, S. K., J. Phys. Mater., vol. **4**, issue 3 (2021) p. 32001.
[4] Shafeeq, S. R., Abdul-Razzaq, M. J., Salim, E., T., Wahid, M. H. A., Key Engineering Materials, vol. **911** (2022) pp. 89-95
[5] Delmdahl, R., Pätzel, R., Applied Physics A, vol. **93** (2008) pp. 611–615 (2008).
[6] Fakhri, M.A., Khalid, F.G., Salim, E.T., Journal of Physics: Conference Series, vol. **1795**, issue 1 (2021) p. 012063
[7] O'Mullane, A. P., Zoolfakar, A. S., Kalantar-Zadeh, K., Austin, M. W., Rani, R. A., J. Mater. Chem. A, vol. **2**, issue 38 (2014) pp. 15683–15703.
[8] Ismail, R. A., Salim, E. T., Halbos, H. T., Optik, vol. **245** (2021) p. 167778
[9] Emeka, N. C., Jen T.-C., P. E. Imoisili, Coatings, vol. **10**, issue 12 (2020) p. 1246.

[10] Salim, E.T., Saimon, J.A., Abood, M.K., Fakhri, M.A, Optical and Quantum Electronics, vol. **52**, issue 10 (2020) p. 463.
[11] Olivares-Navarrete, R. C., Rodil, R. S. E., J. Mater. Sci. Mater. Med., vol. 32, issue 3 (2021) pp. 1–6.
[12] Salim, E.T., Ismail, R. A., Halbos, H. T., Appl. Phys. A, vol. **126** (2020) p. 891.
[13] Lima, A. d., Samuel, C. P., Bergmann, C. L., Collares, F. T., Petzhold, G. B., Leitune, S. M., Werner,V. C. B., J. Dent., vol. **41**, issue 2 (2013) pp. 106–113.
[14] Mahdi, R. O., Fakhri, M. A., Salim, E. T., Materials Science Forum, vol. **1002** (2020) pp. 211-220.
[15] Chen P.-C., Ryu, K., Shen, G., Zhou, C., J. Mater. Chem., vol. **19**, issue 7 (2009) pp. 828–839.
[16] Asady, H., Ismail, R., Salim, E., in AIP Conference Proceedings, vol. **2213**, issue 1 (2020) p. 20183.
[17] Brennaman, M. K., Edward, T., Samulski, Ghosh, R., Lopez, Uher, T., ACS Appl. Mater. Interfaces, vol. **3**, issue 10 (2011) pp. 3929–3935.
[18] Salim, E. T., Saimon, J. A., Abood, M. K., Fakhri, M. A., Mater. Res. Express, vol. **6**, issue 12 (2019) pp. 126459
[19] RobáLee, G., J., Mater. Chem., vol. 1, issue **3** (1991) pp. 381–386.
[20] Fakhri, M.A., Abdulwahhab, A.W., Dawood, M.A., Raheema, A.Q., Numan, N.H., Khalid, F.G., Salim, E.T., International Journal of Nanoelectronics and Materials **11**, (Special Issue BOND21), (2018) pp. 103-108
[21] Chowdari, B. V. R , Jose, R., Le Viet, A., Ramakrishna, S., Reddy, M. V, J. Phys. Chem. C, vol. **114**, issue 1 (2010) pp. 664–671.
[22] Khalid, F. G., Ibraheam, A. S., Fakhri, M. A., Numan, N. H., AIP Conference Proceedings, vol. **2213**, issue 1 (2020) p. 020204.
[23] Lima, A. d., Samuel, C. P., Bergmann, C. L., Collares, F.T., Petzhold, G. B., Leitune, Werner, S. M., Leitune V. C. B.," Int. Endod. J., vol. **46**, issue 3 (2013) pp. 205–210.
[24] Mahmood, R. S., Abdulsatar, W., Fakhri, M. A., AIP Conference Proceedings, vol. **2213**, issue 1 (2020) p. 020236.
[25] Duhn, C. W., Hara, A. T., K. Yi, Karlinsey, R. L., Biomed. Mater., vol. **1**, issue 1 (2006) p. 16.
[26] Alghurabi, M. N. A. K., Mahmood, R. S., Salim, E.T., Alhasan, S.F. H., Khalid, F.G., Materials Today: Proceedings, vol. **42** (2021) pp. 2497-2501
[27] Lin, J., Munir, K. S., Wen, C., Y., Li, Bioact. Mater., vol. **1**, issue 2 (2016) pp. 127–131.
[28] Abdul-Hamead, A. A., Othman, F. M., Fakhri, M. A., Journal of Materials Science: Materials in Electronics, vol. **32** (2021) pp. 15523–15532.
[29] Fu, Z., Kong, J., Qin, Q., J. Electrochem. Soc., vol. **146**, issue 10 (1999) p. 3914.
[30] Abdul-Amir, H.A.A., Fakhri, M.A., Alwahib, A A., Materials Today: Proceedings, vol. 42, (2021) pp. 2815-2821.
[31] Basel, S., Numan, N. H., Khalid, F. G., Fakhri, M. A., AIP Conference Proceedings, vol. **2213**, issue 1(2020) p. 020228
[32] Fakhri, M.A., Basheer, R.A., Banoosh, A.M., Azeez, H.N., Digest Journal of Nanomaterials and Biostructures, vol.**16**, issue 2 (2021) pp. 367-375.
[33] Parveen, B., Naseem, S., Riaz, S., Khalid, Z., J. Appl. Res. Technol., vol. **15**, issue 2 (2017) pp. 132–139.
[34] Mohammed, L. Z., Fakhri, M. A., Abass, A. K., Journal of Physics: Conference Series, vol. **1795**, issue 1 (2021) p. 012055
[35] Langenbeck, P., Appl. Opt., vol. **9**, issue 9 (1970) pp. 2053–2058.
[36] Taleb, S. M., Fakhri, M. A., Adnan, S. A., AIP Conference Proceedings, vol. **2213**, issue 1 (2020) p. 020234
[37] Ntwaeaborwa. O. M., Ogugua, S. N, Swart, H. C., Coatings, vol. **10**, issue 11 (2020) p. 1078.

[38] Fakhri M., Hashim U., Salim E., Tareq, Z., in AIP Conference Proceedings, vol. **2213**, issue 1 (2020) p. 20230.
[39] Menth. A., Tauc, J., J. Non. Cryst. Solids, vol. 8, (1972) pp. 569–585.
[40] Alsultany, F.H., Alhasan, S.F.H. & Salim, E.T., J Inorg Organomet Polym, vol. **31**(2021) pp. 3749–3759.
[41] Baladi, A., Mamoory, R. S., in International Journal of Modern Physics: Conference Series, vol. **5** (2012) pp. 58–65.
[42] Hassan, N. K., Fakhri, M. A., Salim, E. T., Hassan, M. A., Materials Today: Proceedings, vol. **42** (2021) pp. 2769-2772.
[43] Günther, D., Horn. I., Guillong, M, Appl. Surf. Sci., vol. **182**, issue 1–2 (2001) pp. 91–102.
[44] Iryo, K., Nishimura, N., Tsuji, M., Tsuji, T., J. Photochem. Photobiol. A Chem., vol. **145**, issue 3 (2001) pp. 201–207.
[45] Taha, J. M., Nassif, R. A., Numan, N. H., Fakhri, M. A., AIP Conference Proceedings, vol. **2213**, issue 1 (2020) pp. 020235.
[46] Ko, E., Weissman, J., Catal. Today, vol. **8**, issue1 (1990) pp. 27–36.
[47] Alhasan, S. F. H., Bader, B. A., Salim, E. T., Materials Today: Proceedings, vol. **42** (2021) pp. 2845-2848.
[48] Eason, R., John Wiley & Sons, (2007).
[49] Hassan, N. K., Fakhri, M. A., Abdulwahhab, A, W., Hashim, U., Key Engineering Materials, vol. **911**(2022) pp. 65-76.
[50] Castillejo, M., Fernandes, J., Garcia, M., Marco, J., Oujja, M., Quesada, A., Rebollar, E., Appl. Surf. Sci., vol. **452** (2018) pp. 19–31.
[51] Salim, E.T., Khalid, F.G., Fakhri, M.A., Mahmood, R.S., Materials Today: Proceedings, vol. **42** (2021) pp. 2422-2425.
[52] Boruah, B., Madras, G., Modak, J.M., Gupta, R., Nanoscale Adv., vol. **1**, issue 7 (2019) pp. 2748–2760.
[53] Alwazny, M. S., Ismail, R. A. & Salim, E. T., Appl. Phys. A, vol. **128** (2022) p. 500.
[54] Arivanandhan, M., Sanjeeviraja, C., Sivakumar, R., Usha, N., Opt. J. Light Electron Opt., vol. **126**, issue 19 (2015) pp. 1945–1950.
[55] Fakhri, M. A., Ismail, R. A., Abass, A. K., Mohammed, L. Z., Alsultany, F. H., Hashim, U., Silicon (2022). https://doi.org/10.1007/s12633-022-01902-5
[56] Anabela. A., Guan, Z., Gudrun, S., Skrodczki, k., J. Phys. Condens. Matter, vol. **31**, issue 10 (2019), p. 105401.
[57] Abed, A. L., Khalef, W. K., Salim, E. T., Journal of Physics: Conference Series, vol. **1795**, issue 1 (2021) p. 012031
[58] Mohsin, M. H., Numan, N. H., Salim, E. T., Fakhri, M. A., Journal of Renewable Materials, vol. 9, issue 9(2021) pp. 1519-1530.
[59] Kadhim, A., Haleem, A., M., Abass, R., H., *Adv. Environ. Biol.*, vol. 10, no. 12 (2016) pp. 43-55